Applied Catalysis B: Environmental 89 (2009) 432–440

Contents lists available at ScienceDirect

Applied Catalysis B: Environmental

journal homepage: www.elsevier.com/locate/apcatb

Adsorption and oxidation of PCP on the surface of magnetite: Kinetic experiments and spectroscopic investigations

Xiaofei Xue [a,b], Khalil Hanna [a,*], Mustapha Abdelmoula [a], Nansheng Deng [b]

[a] Laboratoire de Chimie Physique et Microbiologie pour l'Environnement (LCPME), UMR 7564 CNRS-Université Henri Poincaré, 405 rue de Vandoeuvre, 54600 Villers-les-Nancy, France
[b] School of Resources and Environmental Science, Department of Environmental Science, Wuhan University, Wuhan 430079, PR China

ARTICLE INFO

Article history:
Received 10 October 2008
Received in revised form 22 December 2008
Accepted 29 December 2008
Available online 15 January 2009

Keywords:
Fenton-like
Oxidation
Adsorption
Magnetite
Mineralization

ABSTRACT

The oxidation of pentachlorophenol (PCP) on the surface of magnetite used as heterogeneous catalyst has been investigated under various experimental conditions (initial substrate concentration, H_2O_2 dose, solid loading and temperature) at neutral pH and correlated with the adsorption behavior. The surface reactivity of magnetite was evaluated by conducting the kinetic study of both H_2O_2 decomposition and PCP oxidation experiments. The occurrence of the optimum values of H_2O_2 and magnetite concentrations for the effective degradation of PCP could be explained by the scavenging reactions with H_2O_2 or iron oxide surface. The surface interactions with PCP in the absence and the presence of oxidant can be well described by Langmuir and Langmuir–Hinshelwood models, respectively. All batch experiments indicate that Fenton-like oxidation of PCP was controlled by surface mechanism reaction and the species compete with each other for adsorption on a fixed number of surface active sites. The apparent degradation rate was dominated by the rate of intrinsic chemical reactions on the oxide surface rather than the rate of mass transfer. Raman analysis suggested that the sorbed PCP was removed form magnetite surface at the first stage of oxidation reaction. The mineralization determined by TOC abatement was completed after 7 d, while total dechlorination was achieved at 4 d treatment time. The first reaction of PCP oxidation should be the dechlorination since 90% of chloride was formed at the first 30 h corresponding to the total disappearance of parent compound. All X-ray powder diffraction (XRD), X-ray photoelectron spectroscopy (XPS), Mössbauer spectroscopy and chemical analyses showed that the magnetite catalyst exhibited low iron leaching, good structural stability and no loss of performance in second reaction cycle.

1. Introduction

Pentachlorophenol (PCP) is a widespread environmental contaminant due to its use for wood preservation and as a pesticide [1,2]. PCP contamination can be found in surface, ground waters and in soils, in the vicinities of past wood-treating facilities [1,2]. The relative resistance of PCP to biological degradation, the reason for its use as a preservative, creates a serious pollution problem [3,4]. Recently, advanced oxidation processes (AOPs) have appeared as a logical alternative to biodegradation [5–7]. These processes based on hydroxyl radical chemistry are currently used for the destruction of organic compounds. The hydroxyl radicals react in a non-selective way on organic compounds leading finally to the mineral end-products. This type of radicals can be easily generated by using hydrogen peroxide and dissolved Fe^{II} (Fenton reagent), but low pH conditions (pH < 4) are required to prevent the precipitation of iron [8]. Unlike the traditional Fenton's reagent, the reaction of Fe-bearing minerals with hydrogen peroxide can effectively oxide the organic molecules at circumneutral pH [9–17]. The Fe^{II}-containing minerals are very interesting in the heterogeneous Fenton reaction, because Fe^{II} play an important role for the initiation of the Fenton reaction according to the classical Haber–Weiss mechanism [9–17]. In this study, magnetite was selected as iron bearing mineral because of its Fe^{II}-structural content and its low solubility in reaction medium [18]. The degradation of PCP by Fenton's reagent [5–7] and Fenton-like system [16] was mainly reported at acidic conditions (pH 3–5). However, information about PCP oxidation at neutral pH is very sparse, and the heterogeneous Fenton degradation of PCP using magnetite at circumneutral pH has been scarcely investigated.

In the Fenton-like system where iron solid mineral was used instead soluble iron, adsorption of the compound and its oxidation by hydroxyl radicals coming from surface-catalyzed reaction could occur simultaneously on the oxide surface. In TiO_2-photocatalysis

* Corresponding author. Tel.: +33 3 83 68 52 42; fax: +33 3 83 27 54 44.
E-mail address: khalil.hanna@lcpme.cnrs-nancy.fr (K. Hanna).

0926-3373/$ – see front matter © 2009 Elsevier B.V. All rights reserved.
doi:10.1016/j.apcatb.2008.12.024

process, the importance of adsorption was widely pointed out in several studies [19–21]. However, the role played by the adsorption at solid surface in the oxidation of pollutant in heterogeneous Fenton reaction is poorly described. Furthermore, the surface interactions of species with iron surface sites involving both sorption and decomposition reactions are scarcely investigated. In this work, the apparent degradation rate of PCP in magnetite/H_2O_2 system was determined under various experimental conditions and correlated with the intrinsic chemical reactions on the oxide surface. For this purpose, the oxidation kinetic was operated at various initial PCP concentration, H_2O_2 dose, magnetite loading and temperature. The Langmuir and Langmuir–Hinshelwood models were used to describe the surface interactions with PCP in the absence and the presence of oxidant, respectively. The surface reactivity of magnetite was evaluated by conducting H_2O_2 decomposition experiments and Raman spectroscopy. The PCP mineralization rate was also determined by monitoring both TOC abatement and chloride formation along the oxidation reaction.

2. Materials and methods

2.1. Chemicals

PCP was procured from Sigma–Aldrich (99% purity) and used as such. Hydrogen peroxide (H_2O_2 35%, w/w) was obtained from Merck.

2.2. Solid characterization

The magnetite sample was purchased from Prolabo (99% purity). In order to identify the crystal structure of mineral, sample of solid was analyzed by X-ray powder diffraction (XRD). The XRD data were collected with a D8 Bruker diffractometer, equipped with a monochromator and a position-sensitive detector. The X-ray source was a Co anode (λ = 0.17902 nm). The diffractogram was recorded in the 3–64° 2θ range, with a 0.0359° step size and a collection of 3 s per point.

The Mössbauer spectra were recorded with MIMOSII, which is designed and fabricated at the university Mainz in Germany [22] and was originally developed for the exploration of the planet Mars. The instrument is operating in backscattering geometry measuring the scattered 14.41 keV Mössbauer radiation and the 6.4 keV Fe X-rays. The main parts of the instrument are the gamma and the X-ray detector, the ^{57}Co Mössbauer source (50 mCi), which is embedded in a rhodium metal matrix attached to a titanium holder, the Mössbauer drive and its control unit and the data acquisition and spectrometer control unit. Four Si-PIN-diodes were selected as detectors to detect backscattered radiation from the sample and was configured to select only 14.4 keV. Measurements were done by placing the detector head against the mylar window of a cell in Plexiglas which contains the sample. The spectra were fitted with the Recoil Software of Lagarec and Rancourt [23], using the Lorentzian model. The parameters resulting from any computer fitting must be mathematically and physically significant (chi^2 minimization).

X-ray photoelectron spectroscopy (XPS) was performed with a KRATOS Axis Ultra X-ray photoelectron spectrometer with a monochromatized Al Kα X-ray source (hn 1/4 486.6 eV) operated at 150 W. XPS is sensitive to the outermost layer of solid sample and provides both semi-quantitative surface composition and chemical state information. In addition, the XPS analysis was very important in verifying the oxidation state of iron at the solid surface.

The specific surface area of magnetite was determined by multipoint N_2-BET analysis using a Coulter (SA 3100) surface area analyzer. The particle size distribution was measured by a dynamic light-scattering method using laser scattering particle size (HARIBA, LA 200). The site density or the concentration of the replaceable surface groups of magnetite was determined by measurement of the amount of fluoride adsorption on the surface [24]. Potentiometric titrations of the oxide were conducted in thermostated double walled pyrex cell at 293 K in 0.001, 0.01 and 0.1 M NaCl solutions according to the method of Parks and Bruyn [25]. The N_2 gas was constantly passed through the suspensions to bubble out the CO_2. The pH value of the suspension was adjusted with titrant solutions (HCl or NaOH) and recorded with the Orion pH meter model 710A having combination glass electrode. The blank titrations were also performed with similar solutions in the absence of the solid. Hence, the estimated pH of zero point of charge, pH_{zpc}, for both iron oxides is close to the value reported in the literature [26]. In addition, the electrophoretic mobility of the particles was measured with a Malvern Zetasizer (NanoZS) as a function of pH in 10 mM NaCl solution and then the zeta potential was calculated from the electrophoretic mobility. The iso-electric point (IEP) of iron oxide is in agreement with the point of zero charge (PZC) determined by potentiometric titration (Table 2). The Fe^{II} content into oxide structure has been determined by chemical analysis after acid dissolution at 60 °C for 48 h. The 6N HCl ensures the dissolution of the iron oxide. Dissolved ferrous iron concentration was measured according to the 1,10-phenanthroline method, using an Agilent 8543 spectrophotometer and fixing λ at 510 nm [27]. Total aqueous iron after dissolution was determined by inductively coupled plasma emission spectroscopy (ICP-AES) (Jobin Yvon-ULTIMA). All chemical analyses were performed in triplicates. Some properties of solid sample are reported in Table 1.

2.3. Sorption experiments

All equilibrium sorption experiments were conducted at 20 °C in the dark at neutral pH. The solid samples were mixed with variable solute concentrations. Results of adsorption kinetic experiments indicated that sorption equilibrium was achieved within 2 h. Before analysis, the suspensions were centrifuged and were filtered through 0.22 μm polyvinylidene fluoride (PVDF) syringe filters (Millipore) that were shown not to sorb PCP. The filtrate samples were analyzed by UV–vis spectroscopy and sorbed concentrations were calculated by difference according to:

$$q_e = \frac{(C_i - C_e)V}{M_s A} \quad (1)$$

where q_e (mmol m^{-2}) is the sorbed concentration, C_e (mmol L^{-1}) is the equilibrium concentration at the end of the experiment, C_i (mmol L^{-1}) is the initial aqueous phase concentration, V (L) is the

Table 1
Physicochemical properties of the investigated magnetite.

Solid	Fe_{tot} (wt%)	Fe^{II}/Fe^{III} ratio	Mean particle diameter (μm)	Specific surface area, SSA ($m^2\ g^{-1}$)	Site density (μmol m^{-2})	Point of zero charge, PZC	Iso-electric point, IEP
Magnetite, Fe_3O_4	70 ± 2	0.48 ± 0.2	4 ± 1	2.4 ± 0.2	3.6 ± 0.2	7.4	7.2

volume of solution, M_s (g) is the mass of solid sorbent, and A ($m^2\,g^{-1}$) is the sorbent specific surface area. The sorption equilibrium experiments were performed in triplicate. The standard deviation of the three replicates was less than 4%.

2.4. Oxidation experiments of PCP

The PCP and the magnetite were stirred for 2 h to ensure the adsorption equilibrium. After this period, 3 mL aliquot was withdrawn to determine the concentration of C_0 and then the oxidant was added to the suspension. The solution pH was adjusted to 7 and kept within 0.1 pH units of this value with diluted solutions of $HClO_4$ and NaOH during the experiments.

During all the oxidation reactions, 3 mL aliquots were withdrawn at selected time intervals, filtered and analyzed. When H_2O_2 was used as an oxidant in the absence of catalyst, oxidation of the starting compound was always negligible. All experimental runs were performed within a temperature of 20 °C in the absence of light. Each experiment was achieved in triplicates. All results were expressed as a mean value of the 3 experiments.

Raman spectroscopy was used to monitor the PCP concentration on the oxide surface in magnetite/H_2O_2 aqueous suspension. Raman spectra were recorded with a triple-subtractive-monochromator Jobin Yvon T64000 spectrometer equipped with a confocal microscope. The detector was a charged-coupled device (CCD) cooled by liquid nitrogen. The Raman spectra were excited by a laser beam at 514 nm emitted by an Argon Laser (Stabilite 2017, Spectra Physics), focused on samples with a diameter of about 0.8 mm and a power of about 2.0 mW on the sample. The Raman backscattering was collected through the microscope objective (100×, numerical aperture of 0.95) and dispersed by a 1800 groves/mm grating to obtain 2.7 cm^{-1} spectral resolution.

2.5. Analytical determinations

The decay of PCP was followed by reversed phase liquid chromatography (HPLC) with a Waters HPLC Detector (486) fitted with a C-18 column (250 mm × 4.6 mm i.d., 5 μm). The mobile phase was a mixture of water/acetonitrile (40:60, v/v) and pH at 3 (using acetic acid). The flow rate of the mobile phase was set at 2.5 mL min^{-1} in the isocratic mode. Detection was carried out at 238 nm. Short chain carboxylic acids were identified and quantified by ion exclusion chromatography fitted with a 300 mm × 6.5 mm i.d. column in conjunction with a Waters UV detector selected at λ = 204 nm. The mobile phase consisted of water containing 290 μg L^{-1} sulfuric acid at a flow rate of 0.6 mL min^{-1}. The aqueous concentration of chloride ions released during oxidation reaction was measured by ion chromatography (Dionex 200), fitted with an anionic exchange column (IonPack AS-14-Dionex) and coupled with a conductivity detector. The mobile phase was a mixture of 3.5 mmol L^{-1} sodium carbonate and 10 mmol L^{-1} sodium hydrogen carbonate solution with a flow rate of 1.2 mL min^{-1}. The injection volume was 20 μL. Total organic carbon was determined with a Shimadzu TOC-5000 Total Organic Carbon Analyzer.

H_2O_2 was measured using the modified *N*,*N*-diethyl-*p*-phenylenediamine DPD method [28]. This method measures H_2O_2 concentrations over the range of 5–50 μmol L^{-1}. Because the H_2O_2 concentrations in the experimental reactors were above this range, each sample was diluted. 0.5 mL of phosphate buffer (pH 6.0) and 5 mL aliquot of diluted sample was mixed in the reaction vial. An aliquot of 50 μL of DPD reagent (3.8×10^{-2} M in 0.1 M H_2SO_4) followed by 50 μL (100 units mL^{-1}) of horseradish peroxidase were then added to reaction vial. The cell was manually shaken for a minute for color development. Absorbance readings were taken at 551 nm using a UV–vis spectrophotometer.

3. Results and discussion

3.1. Characterization of solid sample

The diffractogram of solid powder are shown in Fig. 1a. Five diffraction peaks at $2\theta = 21.2°, 35°, 41.2°, 50.4°$ and 62.8° are shown in the XRD diffractogram, which could be assigned to Fe_3O_4, magnetite [18]. The *d*-space values of theses main peaks were 2.53, 2.96, 2.09, 4.85 and 1.71 Å which may correspond to the more intense lines 3 1 1, 2 2 0, 4 0 0, 1 1 1 and 4 2 2, respectively of magnetite [18].

Magnetite (Fe_3O_4) is the only pure oxide of mixed valence. At room temperature (RT) it has a cubic spinel structure with iron in both tetrahedral and octahedral sites. It is usually represented by the formula $(Fe^{3+})_{tet}[Fe^{3+}Fe^{2+}]_{oct}O_4$. Its Mössbauer spectrum at RT is constituted by a superposition of two subspectra associated to the distribution of the iron in the octahedral and tetrahedral sites. The two valence states on octahedral sites are not distinguishable

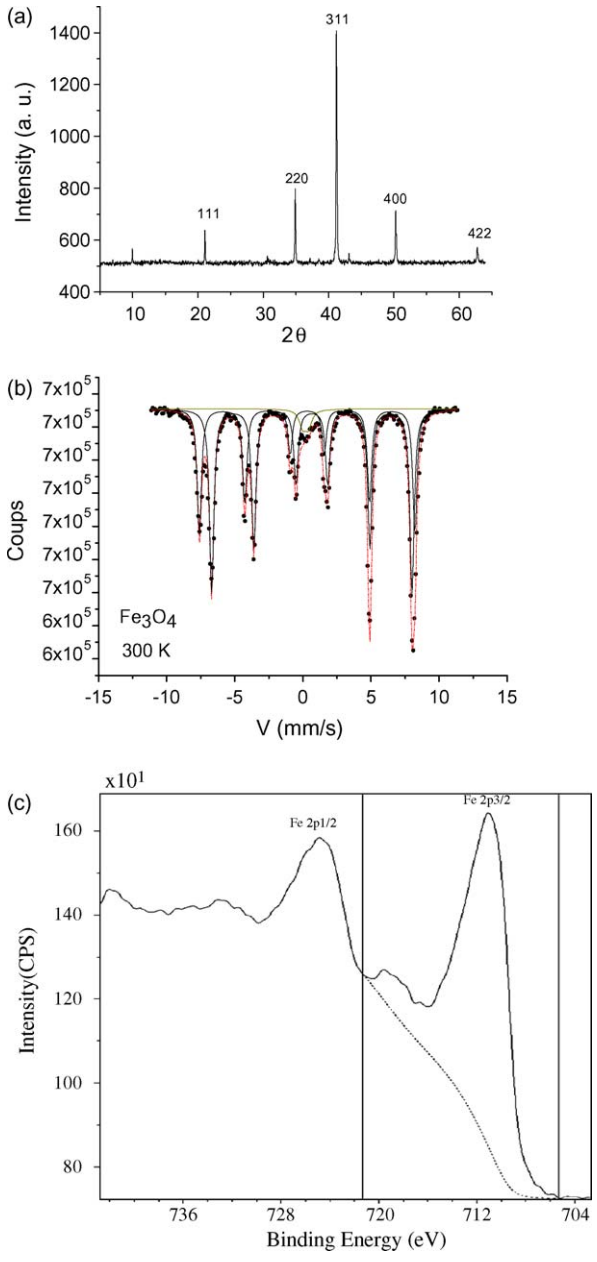

Fig. 1. XRD (a), Mössbauer (b) and XPS (c) spectra of solid sample.

Table 2
Hyperfine parameters of magnetite at room temperature. δ (mm s^{-1}): isomer shift (relative to room temperature α-iron foil); H (kOe): magnetic hyperfine field; Δ or ε (mm s^{-1}): quadrupole splitting or quadrupole shift; RA (%): relative area.

Sample	Component	δ (mm s^{-1})	Δ or ε (mm s^{-1})	H (kOe)	RA (%)
Before reaction	D	0.32	0.3		2.3
	S1	0.31	0	490	38.8
	S2	0.66	0	456	58.9
After reaction	D	0.4	0.47		1.6
	S1	0.31	0	492	39.9
	S2	0.66	0	457	58.5

(valence $Fe^{2.5+}$) due to a fast electron hopping between Fe^{2+} and Fe^{3+} in octahedral sites. Thus, the ideal magnetite has only two distinct sextets at RT [29] in 1:2 intensity ratio corresponding to tetrahedral iron (A sites) with H (magnetic hyperfine field) = 498 - kOe, isomer shift δ = 0.31 mm s^{-1}, and octahedral iron (B site) with H = 465 kOe and δ = 0.67 mm s^{-1}. In our sample, the Mössbauer spectrum at RT (Fig. 1b) has been adjusted with two sextets and their resulting hyperfine parameters (Table 2) are in agreement with literature values for magnetite [30]. The relative area ratio of the two spectral components is close to 1:1.5; it is not exactly 1:2 as would be expected in the stoichiometric magnetite. Otherwise the Mössbauer spectrum shows in the central part a ferric doublet which accounts for 2% of the total absorption and its origin could not be established. Storage of the sample for many years without any particular protection against oxidation could explain the ferric doublet observed in the central part of the spectrum.

The XPS spectrum of the solid material was taken over the entire energy range (data not shown). A detail of the Fe peaks (Fe $2p_{1/2}$ and Fe $2p_{3/2}$) can be seen in Fig. 1c. Deconvolution of the Fe $2p_{3/2}$ peak shows only those corresponding to Fe^{III} component, indicating that the outermost surface of solid sample is already oxidized. This may be probably due to the conditions storage of this commercial sample. It should be noted that XPS is sensitive to the outermost layer of sample, while the Mössbauer spectroscopy detects the iron state in the bulk solid. Some surface properties of solid sample are reported in Table 1.

3.2. Sorption of PCP

Sorption isotherms were determined to investigate the effect of contaminant sorption on the catalytic oxidation (Fig. 2). The experimental isotherm data were fitted to the equations of Langmuir, Freundlich and Tempkin by applying linear regression analysis. One way to asses the goodness of fitting the experimental isotherm data to these equations is to perform an analysis of variance (ANOVA) with error calculation. On the basis of the statistic analysis, the curves were shown a best fit with Langmuir model. The linear form of the Langmuir equation is given by:

$$\frac{C_e}{q_e} = \frac{1}{K_a q_m} + \frac{1}{q_m} C_e \quad (2)$$

where q_m (mmol m^{-2}) is Langmuir maximum sorbed amount and K_a (L $mmol^{-1}$) is the Langmuir isotherm constant. An increasing in PCP concentration showed a progressive saturation of the surface sites. The Langmuir isotherm constants obtained by plotting C_e/q_e against C_e are q_m = 0.023 mmol m^{-2} and K_a = 10.5 L $mmol^{-1}$. The Langmuir maximum sorbed amount is 6 times greater than the site density of solid (Table 1), supposing that more than one molecule might be fixed per iron site (i.e. solute aggregation at oxide surface). A hydrophobic adsorption directly to the iron surface does not seem likely since this is presumed to yield an almost linear isotherm [31]. However, the lack of resistance to desorption when methanol was used to remove the solute sorbed from solid, may signify some hydrophobic interactions rather than a strong phenolate–Fe bond. Kung and McBride [32] reported that while a chemisorption of monochlorophenol (CP) onto goethite (inner-sphere complexation) was identified from FTIR spectroscopy, the mechanism of PCP sorption cannot be easily described.

3.3. Effect of H_2O_2 dose on PCP degradation

Hydroxyl radical can be generated by the reaction between hydrogen peroxide and iron surface leading to PCP degradation. The degradation of organic compounds by $HO^\bullet$ is typically described as a second-order reaction:

$$\frac{d[PCP]}{dt} = -k[PCP][HO^\bullet] \quad (3)$$

where $[HO^\bullet]$ is steady-state concentration of hydroxyl radical, [PCP] is concentration of PCP in water, k is the second-order rate constant, and t is the reaction time. By assuming that $HO^\bullet$ instantaneous concentration is constant, the kinetics of degradation of PCP in water can be described according to the pseudo-first-order equation as given below:

$$[PCP]_t = [PCP]_0 \exp(-k_{app} t) \quad (4)$$

where k_{app} is the pseudo-first-order apparent rate constant (h^{-1}). The k_{app} constants were obtained from the slopes of the straight lines by plotting $-\ln(C_t/C_0)$ as a function of time t, through regression.

The kinetic constants rate k_{app} were determined at different H_2O_2 concentrations (Fig. 3). Since the PCP degradation is directly related to the concentration of the hydroxyl radicals produced by the catalytic decomposition of hydrogen peroxide, more PCP

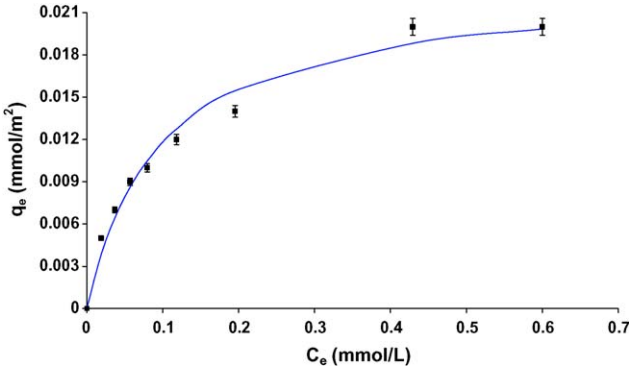

Fig. 2. Sorption isotherm of PCP at pH 7. Solid line represents Langmuir model.

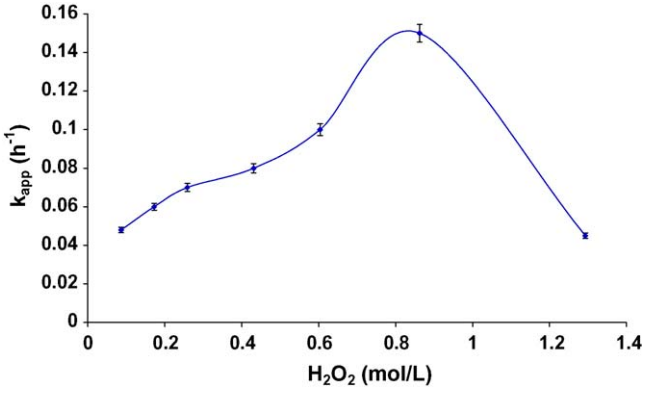

Fig. 3. Degradation kinetic constant of PCP versus H_2O_2 dose. [PCP] = 50 mg L^{-1}, [Magnetite] = 2 g L^{-1}, 20 °C, and pH 7.

decomposition is expected when hydrogen peroxide dosage increases. However, a decrease in the values of k_{app} was observed at a much higher H_2O_2 concentration (Fig. 3). The occurrence of this maximum H_2O_2 concentration for the effective degradation of PCP could be explained by the scavenging effect of hydroxyl radicals by hydrogen peroxide. Similar observation was noted earlier for the degradation of organic compounds by Fenton-like reactions using goethite as catalyst [33]. The HO• radicals preferentially attack the PCP molecules at low H_2O_2 concentration, whereas at much higher H_2O_2 concentration, there is a competitive reaction between the PCP and H_2O_2. The •OH radical may react with hydrogen peroxide producing superoxide/hydroperoxy radicals according to:

$$^{\bullet}OH + H_2O_2 \rightarrow HO_2^{\bullet}/O_2^{\bullet -} + H_2O \quad (5)$$

Buxton et al. [34] have determined the reaction rate of H_2O_2 with hydroxyl radical ($k = 2.7 \times 10^7\ M^{-1}\ s^{-1}$). Because the p$K_a$ of $HO_2^{\bullet}/O_2^{\bullet -}$ is 4.8, generation of hydroperoxide anion $HO_2^{\bullet}$ may be neglected at neutral pH. The generated radicals $O_2^{\bullet -}$ are much less reactive and do not contribute to any oxidation of organic compound [9].

3.4. H_2O_2 decomposition and PCP removal versus exposed surface area per unit volume

The H_2O_2 decomposition was monitored versus time at various exposed surface area of magnetite per unit volume. Good linear plot obtained with the expressions of $\ln([H_2O_2]/[H_2O_2]_0)$ as a function of the reaction time, indicates that the H_2O_2 decomposition is the first order reaction:

$$\frac{d[H_2O_2]}{dt} = -k_{app}[H_2O_2] \quad (6)$$

where k_{app} = [SSA]; [SSA] means the amount of specific surface area (BET method) per unit volume ($m^2\ L^{-1}$). The H_2O_2 decomposition rate k_{app} (min^{-1}) was plotted as a function of [SSA] (Fig. 4a). The good linear relationship ($R^2 = 0.99$) between the rate constant and [SSA] indicates that the H_2O_2 decomposition is the first order reaction with oxide surface area. The results clearly indicate that this is the surface reaction because the increase of surface area provides more active sites for catalytic oxidation. The second-order rate constant (k) obtained from the plot of observed first-order rate constant for H_2O_2 decomposition versus [SSA] is $3 \times 10^{-4}\ min^{-1}(m^2\ L^{-1})^{-1}$.

The PCP degradation was also investigated at various [SSA]. A plot of observed first order rate constant k_{app} (h^{-1}) for PCP removal as a function of [SSA] is shown in Fig. 4a. In contrast with the result of H_2O_2 decomposition rate versus [SSA], the PCP removal was not proportional to the oxide surface area. The observed first order rate constant for PCP oxidation firstly increased with [SSA] increasing and then reduced. This phenomenon can be explained from the assumption that OH radical generated by the reaction between hydrogen peroxide and iron oxide is scavenged by iron surface. Miller and Valentine [35] reported that OH radical is very reactive with natural iron oxide-coated sand ($k = 8 \times 10^{11}\ (g\ mL^{-1})^{-1}\ s^{-1}$).

Oxidation efficiency can be assessed by the following equation:

$$E\ (mol/mol) = \frac{\Delta[PCP]}{\Delta[H_2O_2]} \quad (7)$$

where E (mol/mol) is the stoichiometry efficiency while Δ[PCP] and $\Delta[H_2O_2]$ represent the variation in molar concentration of PCP and H_2O_2 as a function of [SSA]. A high E value means a high reaction yield between PCP and hydroxyl radicals. Fig. 4b shows that PCP oxidation efficiency increased with [SSA] increasing and then reduced. At low [SSA], the generated HO• radicals preferentially react with PCP molecules, whereas at high [SSA], the iron surface can act as an OH radical scavenger.

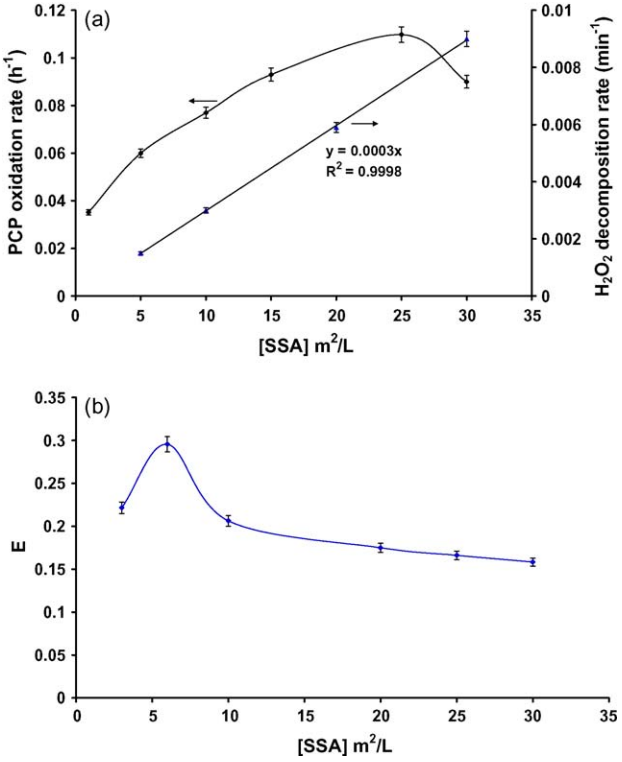

Fig. 4. (a) Degradation kinetic constant of PCP and H_2O_2 decomposition rate versus [SSA]. (b) Oxidation efficiency (E) versus SSA. [PCP] = 50 mg L^{-1}, [H_2O_2] = 150 mM, 20 °C, and pH 7 for the PCP degradation. [H_2O_2] = 1 mM, 20 °C, and pH 7 for H_2O_2 decomposition.

3.5. Effect of initial PCP concentration

The pseudo-first-order apparent rate constant was determined at various initial PCP concentration (Fig. 5). The pseudo-first-order degradation rate constant of PCP decreased when the initial concentrations of PCP increased from 10 to 100 mg L^{-1}. Increased amount of pollutant may occupy a greater number of iron active sites, which become unavailable for H_2O_2 and result in lower HO• generation rate. More PCP sorbed on the magnetite surface and less H_2O_2 interacted with iron surface and so less hydroxyl radical formed at the surface. These results are consistent with many photocatalysis studies where activation by photon absorption is typically the first step for reaction; reaction rates were lowered with the higher initial concentration [19–21,36]. The Langmuir–Hinshelwood model that is widely used in heterogeneous catalysis was tested [20,36]. In this case, the species present in the reaction compete with each other for adsorption on a fixed number of active sites. This Langmuir–Hinshelwood model postulates that the rate of reaction of two species adsorbed on the surface is the rate-limiting step:

$$k_{app} = \frac{k_{int}K_s}{1 + K_s[PCP]_i} \quad (8)$$

and linear expression:

$$\frac{1}{k_{app}} = \frac{1}{k_{int}}[PCP]_i + \frac{1}{k_{int}K_s} \quad (9)$$

where k_{app} is the initial pseudo-first-order rate constant (h^{-1}), k_{int} is the intrinsic reaction rate constant (mmol $L^{-1}\ h^{-1}$), and K_s is the

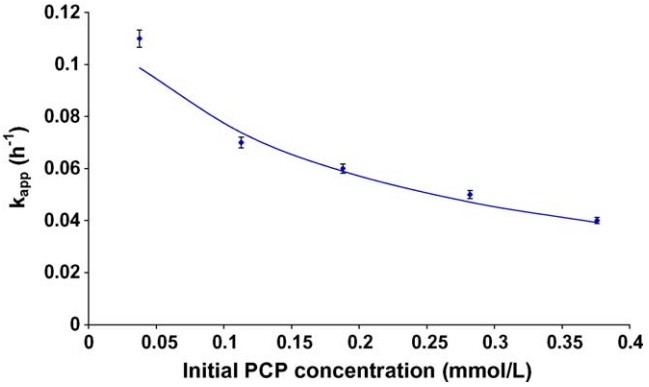

Fig. 5. Degradation kinetic constant of PCP versus initial concentration of PCP. [Magnetite] = 2 g L^{-1}, H_2O_2 = 150 mM, 20 °C, and pH 7. Solid line represents Langmuir–Hinshelwood model.

adsorption constant of PCP over magnetite surface (L $mmol^{-1}$). The linear correlation ($r^2 \sim 0.98$) between $1/k_1$ and $[PCP]_i$ is relatively good, indicating that surface reactions of PCP including sorption and oxidation by surface •OH, play an important role in determining rate of the whole reaction. k_{int} and K_s were obtained as 0.022 mmol L^{-1} h^{-1} and 5.40 L $mmol^{-1}$. This K_s value is lower than the sorption constant determined in the absence of oxidant by Langmuir model, suggesting an adsorption competition for the magnetite surface.

In order to verify the competition between species and the implications of iron surface sites in the decomposition of these species, H_2O_2 decomposition and PCP oxidation experiments are operated in the presence of fluoride ions at pH 7. Magnetite and fluoride solution were stirred for 1 h to reach equilibrium sorption, after that H_2O_2 or PCP was added. Fluoride exhibits a strong chemical affinity for iron oxide surfaces and is capable of forming both inner and/or outer sphere complexes with iron oxide surfaces, with an intrinsic surface complexation constant of $\log K_{int} = 9.3$ [37]. This might reduce the surface sites available for chemically specific interactions with H_2O_2 or PCP, and lead to inactivation of iron mineral surfaces. Coherently, decrease in H_2O_2 decomposition rate value was observed with fluoride (Fig. 6a).

The observed decrease in PCP oxidation rate in the presence of fluoride (F^-) (Fig. 6b) may be due to several factors: (i) the decrease in H_2O_2 decomposition rate and so decrease in hydroxyl radical generation rate, (ii) the decrease in PCP sorption rate because of the competition with F^- for adsorption on surface active sites or (iii) the scavenging effect of fluoride ions towards hydroxyl radical in solution. Batch experiments showed that the presence of fluoride resulted in PCP adsorption decreasing on magnetite (around 50%). Furthermore, the scavenging of hydroxyl radical by chloride or fluoride is operational in acidic solution only and not at neutral to basic pH [38]. The increase of fluoride concentration to 1 mM did not significantly reduce more the oxidation performance observed at 0.1 mM, corroborating that the scavenging effect of hydroxyl radical by fluoride is not significant under our experimental conditions. These observations confirm that the Fenton-like oxidation of PCP is controlled by surface mechanism reaction and adsorption of H_2O_2 or PCP on the surface of magnetite can affect the whole degradation reaction rate.

3.6. Mass transfer rate of species

The apparent rate of a heterogeneous reaction is usually dominated by either the rate of intrinsic chemical reactions on the surface or the rate of diffusion of the solutes to the surface. Since the solid used in this study was not porous, the diffusion rate

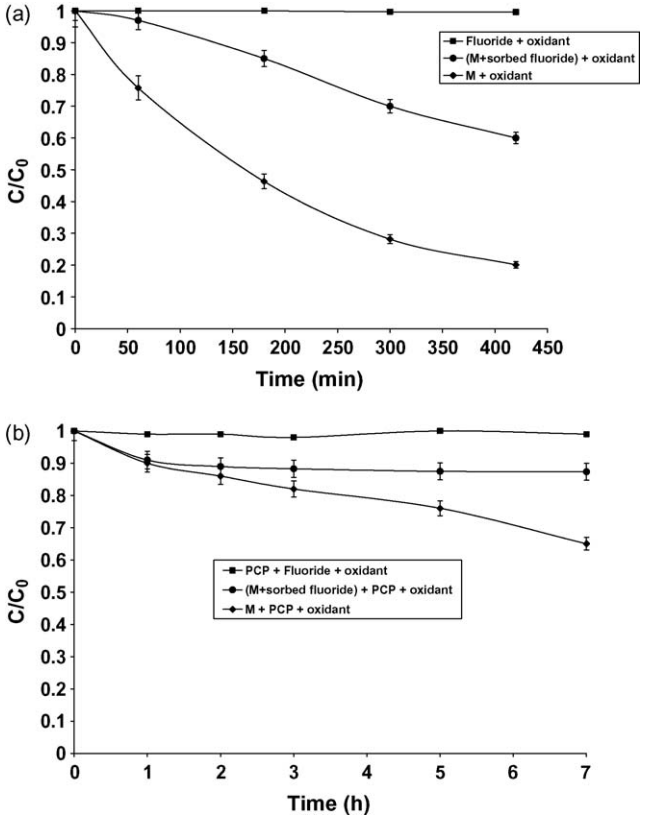

Fig. 6. (a) H_2O_2 decomposition versus time after F^- sorption and (b) PCP removal versus time after F^- sorption. [H_2O_2] = 1 mM, F^- = 0.1 mM, [Magnetite (M)] = 10 m^2 L^{-1}, 20 °C, and pH 7 for H_2O_2 decomposition. [Magnetite (M)] = 2 g L^{-1}, H_2O_2 = 150 mM, F^- = 0.1 mM, 20 °C and pH 7 for the PCP degradation.

through the liquid film (external mass transfer resistance) was only considered.

Assuming that the entire surface is equally accessible, the rate of flow of substrate to the surface has been found to be proportional both to the surface area (A) and the difference in substrate concentration ([S]) between the bulk of the solution and the microenvironment next to the surface. The mass transfer coefficient k (cm s^{-1}) which depends upon the diffusivity of the substrate and the effective distance between the surface and the bulk phase can be written as:

$$k = \frac{D}{L} \tag{10}$$

D is the diffusion coefficient (cm^2 s^{-1}) and L is the thickness of the stagnant liquid film (cm).

The rate of diffusion can be expressed as:

$$\alpha = \frac{D}{L^2} \tag{11}$$

The diffusion coefficient of the solutes in liquids is typically $\sim 10^{-5}$ cm^2 s^{-1}, and the stagnant layer thickness of the liquid film can be estimated by the Film theory as $\sim 10^{-3}$ cm [39]. So, the mass transfer coefficient was estimated as 10^{-2} cm s^{-1} and the rate of diffusion as 10 s^{-1}.

The maximum observed rate for the PCP oxidation and for the decomposition of hydrogen peroxide is $\sim 3.8 \times 10^{-5}$ s^{-1} and 1.5×10^{-4} s^{-1}, respectively. So, the rate of diffusion is much faster than the reaction rate of either H_2O_2 or PCP on the iron oxide surface. Furthermore, the intrinsic reaction rate constant determined by Langmuir–Hinshelwood model was 6.1×10^{-6} mmol L^{-1} s^{-1}.

Therefore, the intrinsic reactions on the oxide surface including sorption and oxidation are expected to be the rate-limiting steps.

The kinetic rate constant of PCP degradation was also determined at different temperatures (10, 20, 30, and 40 °C) to determine the activation energy of the PCP oxidation on the oxide surface ([PCP] = 50 mg L^{-1}, [Magnetite] = 2 g L^{-1}, H_2O_2 = 0.8 M, pH 7). A correlation can be established by plotting the data from temperature and kinetic degradation rate (k_{app}) using linear form of Arrhenius equation:

$$\ln k_{app} = \ln A + \left(\frac{-E_a}{RT}\right) \quad (12)$$

where A is a constant and E_a is the activation energy. The activation energy of the reaction was determined as 47 ± 3.2 kJ mol^{-1}. This value is close to that reported by Seung et al. [40] for the oxidation activation energy of PCP in supercritical water (43.56 ± 1.47 kJ mol^{-1}).

The activation energy value of PCP degradation is higher than that of the diffusion-controlled reactions, which usually ranges within 10–13 kJ mol^{-1} [41]. These results corroborates that the apparent reaction rate is dominated by the rate of intrinsic chemical reactions on the oxide surface rather than the rate of mass transfer.

3.7. Removal of PCP in aqueous or sorbed phase

The interactions between oxidant and iron surface can be explained by heterogeneous reactions analogous to the solution phase reactions [42–44], where the dominant reaction is first a chain of reactions occurring on the mineral surface:

$$\equiv Fe^{II} + H_2O_2 \rightarrow \equiv Fe^{III} + HO^- + HO^\bullet \quad (13)$$

$$\equiv Fe^{III} + H_2O_2 \rightarrow \equiv Fe^{III}(H_2O_2) \quad (14)$$

$$\equiv Fe^{III}(H_2O_2) \rightarrow (\equiv Fe^{II}{}^\bullet O_2H) + H_2O \quad (15)$$

$$(\equiv Fe^{II}{}^\bullet O_2H) \rightarrow \equiv Fe^{II} + HO_2^\bullet/O_2^{\bullet -} \quad (16)$$

$HO_2^\bullet/O_2^{\bullet -}$ plays an important role in the redox cycle of iron in aqueous phase and generates oxygen as a by-product but the interactions of superoxide/hydroperoxy radicals with the iron mineral surface are not yet well argued:

$$\equiv Fe^{III} + O_2^{\bullet -} \rightarrow \equiv Fe^{II} + O_2 \quad (17)$$

$$\equiv Fe^{II} + HO_2^\bullet/O_2^{\bullet -} \rightarrow \equiv Fe^{III} + HO_2^- \quad (18)$$

Other competitive reactions may occur such as the auto-decomposition of H_2O_2 to oxygen and water, the recombination of OH radicals to generate H_2O_2. However, the disproportionation of hydroperoxy radical (combination of two hydroperoxy radicals to H_2O_2 and O_2) is not expected because generation of hydroperoxide anion $HO_2^\bullet$ may be neglected at neutral pH.

On the other hand, the interactions between PCP and iron surface sites (≡Fe) can be described as equilibrium reaction between sorbed and aqueous species:

$$\equiv Fe + PCP_e \leftrightarrow \equiv Fe(PCP)_s \quad (19)$$

The hydroxyl radicals formed by the reaction between hydrogen peroxide and iron surface can probably attack the sorbed species as well as the aqueous species leading to the degradation and mineralization of PCP:

$$HO^\bullet + \equiv Fe(PCP)_s \rightarrow \equiv Fe + (\text{PCP by-products})_{solution} \rightarrow Cl^- + CO_2 \quad (20)$$

$$HO^\bullet + PCP_e \rightarrow \text{PCP by-products} \rightarrow Cl^- + CO_2 \quad (21)$$

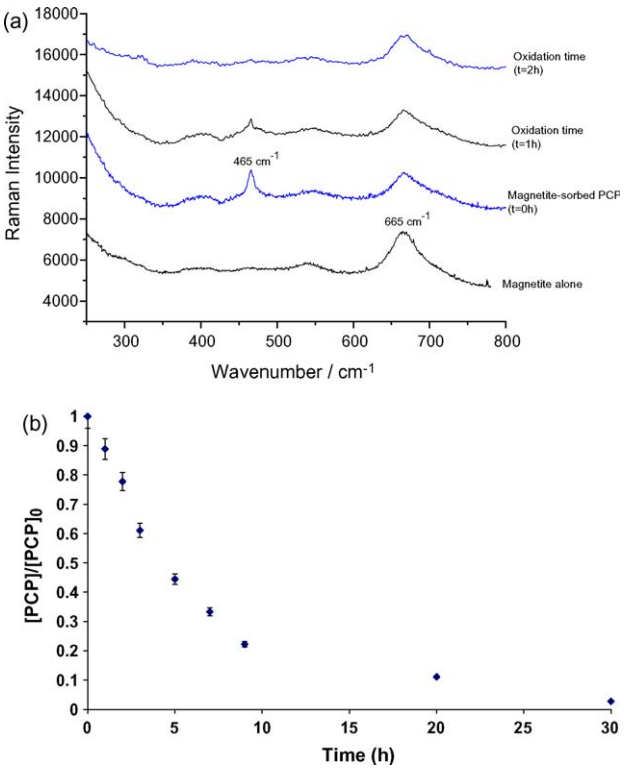

Fig. 7. (a) Raman spectra of sorbed PCP on magnetite before and after exposure to H_2O_2. (b) PCP decay versus time. [PCP] = 50 mg L^{-1}, [Magnetite] = 2 g L^{-1}, H_2O_2 = 0.8 M, 20 °C, and pH 7.

Raman spectra show the PCP sorbed on the surface of magnetite along the oxidation reaction (Fig. 7a). Prior to Raman analysis, oxidation experiment of PCP at neutral pH was conducted versus time in 2 g L^{-1} of magnetite with the optimum value of H_2O_2 dose (Fig. 7b). During the oxidation reaction, a few milligrams of magnetite were sampled from oxidation reactor at selected time intervals and immediately analyzed by Raman spectroscopy without drying (Fig. 7a). The PCP amount was also quantified in aqueous phase and in solid phase after extraction by chromatography analysis.

Based on the Raman signature, the band at 665 cm^{-1} could be assigned to magnetite (Fe_3O_4) [45], while the stronger band of PCP is around 465 cm^{-1} (Fig. 7a). The sorbed PCP disappeared from the surface of magnetite at 2 h treatment time before the total removal of PCP in aqueous solution (occurred at around 30 h as shown in Fig. 7b). Both degradation and desorption processes could explain the disappearance of PCP from magnetite surface at the first stage of reaction. In the case of degradation, the OH radicals generated from the surface reaction between hydrogen peroxide and surface active sites may preferentially react with surface sorbed PCP. In the case of desorption, H_2O_2 competed with PCP for the fixation on magnetite active sites as previously shown by Langmuir–Hinshelwood model, and displaced it from surface to aqueous phase.

3.8. Kinetic of PCP mineralization

The PCP mineralization was determined by both TOC and chloride formation measurements (Fig. 8). The first reaction of PCP oxidation should be the dechlorination since 90% of chloride was formed at the first 30 h corresponding to the total disappearance of parent compound (Fig. 7b). Total dechlorination (chloride mass balance corresponding to 50 mg L^{-1} of PCP) was achieved at 4 d treatment time and complete mineralization measured by TOC abatement occurred after 7 d. The remained TOC after total

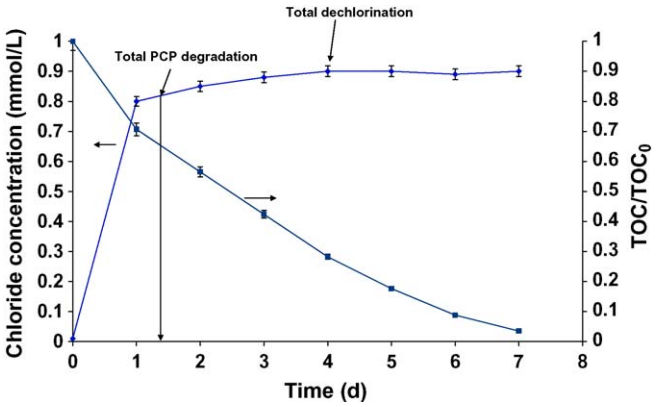

Fig. 8. TOC abatement and chloride formation versus time. [PCP] = 50 mg L^{-1}, [Magnetite] = 2 g L^{-1}, H_2O_2 = 0.8 M, 20 °C, and pH 7.

dechlorination at 4 d (28%), 5 d (18%) and 6 d (10%) could be attributed to organic acids accumulated in the solution. In order to identity the end-products, aliquots sampled at 4 d, 5 d and 6 d treatment times were analyzed by ion exclusion chromatography (results not reported). Two major peaks corresponding to oxalic acid and formic acid were identified by comparison of their retention time with those of authentic standards. Note that oxalic and formic acids have been well described as by-products of the aromatic ring cleavage and often detected in solution after Fenton treatment [7,17].

In order to confirm the role played by •OH in the degradation of PCP in the Fenton-like reactions, the reaction with magnetite was repeated with the addition of excess 2-propanol as an •OH scavenger. 2-Propanol is rapidly oxidized by hydroxyl radicals ($k_{OH\bullet} = 3 \times 10^9\ M^{-1}\ s^{-1}$) but is less reactive with superoxide $O_2^{\bullet-}$ ($k_{O_2\bullet^-} = 1 \times 10^6\ M^{-1}\ s^{-1}$) [46]. Addition of 2-propanol (2%, v/v) in the magnetite/H_2O_2 system inhibited the oxidation of PCP which confirms the predominant role of hydroxyl radical in the dechlorination and mineralization of PCP and corroborates with a Fenton-like reaction taking place in this system.

3.9. Structural and catalytic stabilities

The action of H_2O_2 on the oxide surface can transform the oxide particles into an only Fe^{III}-bearing mineral or into an amorphous iron oxide which may be less stable and more soluble. This mineralogical transformation may lead to a substantial change in the surface characteristics of the mineral, causing a different kinetic behavior and decomposition rate for H_2O_2. The very low dissolved iron concentration measured (<0.05 mM) did not expect the formation of more soluble iron oxide. The chemical analyses of the solid after reaction revealed no significant change in the total Fe loading. In addition, XRD diffractogram recorded at the end of oxidation reaction was found to be similar to that recorded before reaction (i.e. Fig. 1a). Furthermore, the hyperfine parameters of Mössbauer spectra shown in Table 2 are unchanged after reaction, indicating a strong structural stability of solid.

The reusability of the solid has been evaluated under identical oxidation conditions as for the first oxidation cycle. At the end of the oxidation process, the solid is easily removed from the reactor, dried in the glovebox under N_2 and stored at ambient temperature. The H_2O_2 decomposition and PCP degradation on the recovered catalyst were then investigated as for previous experiments and showed a slight difference with the first oxidation cycle. Indeed, k_{app/H_2O_2} and $k_{app/PCP}$ are found to be respectively 0.058 h^{-1} and 0.0040 min^{-1} for the first batch oxidation, and 0.060 h^{-1} and 0.0039 min^{-1} for the second oxidation cycle. So, no deactivation of surface catalytic sites was caused by the adsorption/oxidation process. The excellent stability of the catalytic activity could be attributed to the low loss of iron content and to the structural stability of magnetite during oxidation cycles at neutral pH. However, the oxidative transformation of magnetite to maghemite and goethite may be possible at high pH conditions as reported by Thomas He et al. [47]. In this work, the authors stated that the possible transformation mechanism of magnetite at alkaline conditions is through the dissolution and re-precipitation process [47].

4. Conclusion

The degradation rate of PCP by Fenton-like oxidation firstly increased with the dosage of H_2O_2 or with the amount of magnetite, reached a maximum value and then decreased. The occurrence of these maximum values for the effective degradation of PCP could be explained by the scavenging reaction with H_2O_2 or iron oxide surface. The PCP mineralization determined by TOC was completed after 7 d, while total dechlorination was achieved at 4 d treatment time. The first reaction of PCP oxidation should be the dechlorination since 90% of chloride was formed at the first 30 h corresponding to the total disappearance of parent compound. The magnetite catalyst exhibited low iron leaching, good structural stability and no loss of performance in second reaction cycle. The apparent reaction rate for heterogeneous Fenton reaction is dominated by the rate of intrinsic chemical reactions on the oxide surface rather than the rate of mass transfer. All batch experiments indicate that Fenton-like oxidation of PCP is mainly controlled by surface mechanism reaction and the species compete with each other for adsorption on a fixed number of magnetite active sites. Raman analysis suggested that the sorbed PCP was removed form magnetite surface at the first stage of oxidation reaction. Due to the complex nature of chemical surface species, it is difficult to fully understand the multiple interactions that occur on the oxide surface. Spectroscopic characterization *in situ* of surface active sites and solute surfaces complexes during the oxidation reaction are required for this purpose.

Acknowledgements

We gratefully acknowledge C. Carteret for his help in Raman analysis, M. Mullet and J. Lambert for XPS analysis and for many helpful discussions with regards to the magnetite structure.

References

[1] K. Schellenberg, C. Leunberger, R.P. Schwarzenbach, Environ. Sci. Technol. 18 (1984) 652–657.
[2] US EPA, EPA/600/R-92/182 US EPA, Washington, DC, 1992.
[3] J.G. Mueller, D.P. Middaugh, S.E. Lantz, P.J. Chapman, Appl. Environ. Microbiol. 57 (1991) 1277–1285.
[4] K.A. McAllister, H. Lee, J.T. Trevors, Biodegradation 7 (1996) 1–4.
[5] M. Fukushima, K. Tatsumi, Environ. Sci. Technol. 35 (2001) 1771–1778.
[6] K. Hanna, Ch. Brauer, P. Germain, J.M. Chovelon, C. Ferronato, Sci. Total Environ. 332 (2004) 51–60.
[7] K. Hanna, S. Chiron, M.A. Oturan, Water Res. 39 (2005) 2763–2773.
[8] H.J.H. Fenton, J. Chem. Soc. 65 (1894) 899–910.
[9] S.S. Lin, M.D. Gurol, Environ. Sci. Technol. 32 (1998) 1417–1423.
[10] R.L. Valentine, H.C.A. Wang, J. Environ. Eng. 124 (1998) 31–38.
[11] R.J. Watts, M.K. Foget, S.H. Kong, A.L. Teel, J. Hazard. Mater. 69 (1999) 229–243.
[12] W.P. Kwan, B.M. Voelker, Environ. Sci. Technol. 36 (2002) 1467–1476.
[13] W.P. Kwan, B.M. Voelker, Environ. Sci. Technol. 37 (2003) 1150–1158.
[14] R. Matta, K. Hanna, S. Chiron, Sci. Total Environ. 385 (2007) 242–251.
[15] K. Hanna, T. Kone, G. Medhagi, Catal. Commun. 9 (2008) 955–959.
[16] R.J. Watts, M.D. Udell, S. Kong, S.W. Leung, Environ. Eng. Sci. 16 (1999) 93–97.
[17] R. Matta, K. Hanna, S. Chiron, Sep. Purif. Technol. 61 (2008) 442–446.
[18] U. Schwertmann, R.M. Cornell, Iron Oxides in the Laboratory: Preparation and Characterization, Wiley-VCH, New York, 2000.
[19] J.M. Herrmann, Catal. Today 53 (1999) 115–129.
[20] D.W. Chen, A.K. Ray, Water Res. 32 (1998) 3223–3234.
[21] N. Daneshvar, M. Rabbani, N. Modirshahla, M.A. Behnajady, J. Photochem. Photobiol. A: Chem. 168 (2004) 39–45.

[22] G. Klingelhöfer, R.V. Morris, B. Bernhardt, C. Shröder, D.S. Rodionov, P.A. de Souza, a. Yen, R. Gellert, E.N. Evlanov, B. Zubkov, J. Foh, U. Bonnes, E. Kankeleit, P. Gutlich, W. Ming, F. Renz, T. Wdowiak, S.W. Squyres, R.E. Arvidson, Science 306 (2004) 1740–1745.
[23] K. Lagarec, D.G. Rancourt, Nucl. Instrum. Meth. B 129 (1997) 266–280.
[24] L. Sigg, W. Stumm, Colloid. Surf. 2 (1981) 101–117.
[25] G.A. Parks, P.L.J. Bruyn, Phys. Chem. 66 (1962) 967–973.
[26] T.J. Daou, S. Begin-Colin, J.M. Greneche, F. Thomas, A. Derory, P. Bernhardt, P. Legare, G. Pourroy, Chem. Mater. 19 (2007) 4494–4505.
[27] H. Tamura, K. Goto, T. Yotsuyanagi, M. Nagayama, Talanta 21 (1974) 314–318.
[28] H. Bader, V. Sturzenegger, J. Hoigné, Water Res. 22 (1988) 1109–1115.
[29] E. Murad, J.H. Johnston, in: G.J. Long (Ed.), Mössbauer Spectroscopy Applied to Inorganic Chemistry, vol. 2, Plenum, New York, 1987.
[30] G.M. Da costa, E. De Grave, P.M.A. De Bakker, R.E. Vandenberghe, Clays Clay Miner. 43 (1995) 656–668.
[31] C.T. Chiou, P.E. Porter, D.W. Schmedding, Environ. Sci. Technol. 17 (1983) 227–231.
[32] K.H.S. Kung, M.B. McBride, Environ. Sci. Technol. 25 (1991) 702–709.
[33] J.J. Wu, M. Muruganandham, J.S. Yang, S.S. Lin, Catal. Commun. 7 (2006) 901–906.
[34] G.V. Buxton, C.L. Greenstock, W.P. Helman, A.B. Ross, J. Phys. Chem. 17 (1988) 513–886.
[35] C.M. Miller, R.L. Valentine, Water Res. 33 (1999) 2805–2816.
[36] D.F. Ollis, N. Serpone, E. Pelizzetti, in: N. Serpone, E. Pelizzetti (Eds.), Photocatalysis Fundamentals and Applications, Wiley, New York, 1989.
[37] D.A. Dzombak, F.M.M. Morel, Surface Complexation Modeling: Hydrous Ferric Oxide, Wiley-Interscience, New York, 1990.
[38] E. Lipczynska-Kochany, G. Sprah, S. Harms, Chemosphere 30 (1995) 9–20.
[39] T.K. Sherwood, R.L. Pigford, C. Wilke, Mass Transfer, McGraw-Hill, New York, 1975.
[40] H.H. Seung, B. Veriansyah, J.D. Kim, J.C. Lee, J. Environ. Sci. Health A 42 (2007) 2105–2109.
[41] W. Stumm, J. Morgan, Aquatic Chemistry, 3rd ed., Wiley-Interscience, New York, 1996.
[42] W.G. Barb, J.H. Baxendale, D. George, K.R. Hargrave, Faraday Soc. Trans. 47 (1951) 591–616.
[43] J.J. Pignatello, Environ. Sci. Technol. 26 (1992) 944–951.
[44] C. Walling, M. Cleary, Int. J. Chem. Kinet. 9 (1977) 595–601.
[45] D. Neff, L. Bellot-Gurlet, P. Dillmann, S. Reger, L. Legrand, J. Raman Spectrosc. 37 (2006) 1228–1237.
[46] A.L. Teel, R.J. Watts, J. Hazard. Mater. 94 (2002) 179–218.
[47] Y. Thomas He, J. Samuel, Traina, Environ. Sci. Technol. 39 (2005) 4499–4504.